# Comparative Analysis of Land Surface Temperature (LST) Retrieved from Landsat Level 1 and Level 2 Data: A Case Study in Pathumthani Province, Thailand

**Thammaboribal, P.,[1*] Tripathi, N. K.[1] and Lipiloet, S.[2]**
[1]Asian Institute of Technology, School of Engineering and Technology, P.O.Box 4, Klong Luang, Pathumthani 12120, Thailand, E-mail: prapasgnss@gmail.com*
[2]Department of Civil Engineering, Faculty of Engineering, Rajamangala University of Technology Thanyaburi, Pathumthani 12120, Thailand
**Corresponding Author*

**DOI: https://doi.org/10.52939/ijg.v21i4.4089**

**Abstract**
*Land Surface Temperature (LST) is a critical parameter for environmental monitoring, urban heat island (UHI) studies, climate research, and sustainable land management. This study presents a comprehensive comparative analysis of LST retrieved from Landsat Level 1 (L1) and Level 2 (L2) data in Pathumthani Province, Thailand, a rapidly urbanizing region. The research aims to evaluate the consistency, reliability, and practical implications of LST values derived from both data processing levels, using multi-temporal imagery from Landsat 5, 7, 8, and 9 acquired between 2004 and 2025. LST was derived from L1 data through a radiative transfer approach combined with NDVI-based emissivity estimation, while L2 data provided pre-processed surface temperature products generated using standardized atmospheric correction algorithms. The results reveal significant discrepancies between the two datasets, with L2-derived LST consistently exhibiting higher values than L1-derived LST by as much as 36.24°C in urban areas. Notably, Landsat 7 L2 data produced extreme LST values (e.g., 82.34°C), which are unrealistic for urban surface temperatures and raise concerns about potential overcorrection in the L2 processing chain. In contrast, L1 data yielded more plausible LST estimates for urban environments but systematically underestimated temperatures over water bodies due to limitations in emissivity assumptions for aquatic surfaces. The study highlights the critical influence of atmospheric correction methods, emissivity modeling, and sensor-specific algorithms on LST accuracy. While L2 products offer convenience as science-ready data, their tendency toward temperature overestimation in urban areas suggests caution in their use for UHI studies and thermal analysis. Conversely, L1 data, when processed with appropriate emissivity corrections, provide more reliable results for built-up landscapes but require additional validation for water bodies. These findings have important implications for researchers, urban planners, and policymakers, emphasizing the need for context-specific data selection in thermal remote sensing applications. The study concludes with recommendations for optimizing LST retrieval methods in heterogeneous environments and underscores the value of integrating multi-source validation data to enhance the accuracy of satellite-derived temperature products in support of climate resilience and sustainable urban development initiatives.*

**Keywords:** Emissivity, Land Surface Temperature (LST), Landsat Level 1 And Level 2, Urban Heat Island

## 1. Introduction

Land Surface Temperature (LST) is a crucial parameter for understanding surface atmosphere energy exchanges, and plays a significant role in a variety of environmental applications. It is particularly important in studies related to climate change, urban heat island effects, land degradation, and water stress. Accurate LST measurements are essential for monitoring thermal characteristics of the Earth's surface, supporting agricultural planning, assessing ecological conditions, and guiding sustainable urban development, especially in rapidly urbanizing regions. Remote sensing provides an effective means for estimating LST, offering consistent spatial and temporal coverage that cannot be easily achieved through ground-based measurements alone.

Among the remote sensing platforms available, the Landsat series is particularly valuable due to its long historical record, moderate spatial resolution, and availability of thermal infrared (TIR) bands suitable for local- and regional-scale analysis. These characteristics have made Landsat data widely used in LST studies over both natural and built-up landscapes.

Studying the Urban Heat Island (UHI) effect is essential due to its significant impacts on public health, energy consumption, and environmental quality. UHI leads to elevated temperatures in urban areas compared to their rural surroundings, increasing the risk of heat-related illnesses, especially during extreme weather events. It also drives higher energy use for cooling, contributing to greater greenhouse gas emissions and air pollution. Moreover, UHI affects local ecosystems and biodiversity while posing challenges for sustainable urban development. Understanding UHI is therefore crucial for designing climate-resilient cities and implementing effective urban planning strategies to mitigate heat stress and promote livability. There are several studies that LST was utilized to investigate the UHI, especially urban hot spots (UHS) [1][2][3] [4][5][6][7] and [8]. Moreover, the relationship between LST and land use land cover (LULC) were also widely investigated [9][10][11] [12] and [13].

Numerous studies have also explored different methodologies and algorithms for retrieving LST from Landsat data using at-sensor radiance and land surface emissivity data. These algorithms are typically tailored to the specific characteristics of individual thermal sensors aboard satellites. For example, A a single-channel algorithm for urban thermal analysis was developed by [14], while the use of NDVI-derived emissivity to enhance LST accuracy was proposed by [15]. As a result, an algorithm designed for one thermal sensor, or a particular combination of thermal sensors cannot be directly applied to others, due to variations in sensor calibration, spectral response, and spatial resolution.

Landsat data are delivered in several processing levels. Level 1 data include radiometrically and geometrically corrected imagery, which requires further atmospheric correction and emissivity estimation to derive LST. In contrast, Level 2 products provide atmospherically corrected surface reflectance and pre-processed LST values using standard algorithms. While both datasets can be used for LST retrieval, differences in the preprocessing chain including atmospheric correction models, radiative transfer assumptions, and emissivity estimation can result in significant discrepancies in LST outcomes.

Recently, [16] demonstrated that Level 2 surface reflectance products improve the precision of LST estimation in heterogeneous landscapes. However, while methodological advancements have been widely documented, few studies have conducted direct comparisons of LST derived from Level 1 and Level 2 Landsat data under the same environmental and geographic conditions [17][18] and [19]. This research aims to fill that gap by comparing LST values derived from Landsat Level 1 and Level 2 products in Pathumthani Province, Thailand a peri-urban area within the Bangkok Metropolitan Region experiencing rapid land-use transformation. By assessing differences in LST outputs from these two data levels, this study seeks to evaluate their consistency and reliability. The findings will support more informed decision-making in selecting appropriate Landsat data products for thermal analysis and environmental monitoring in similar urbanizing contexts.

## 2. Methodology

The methodology of this study focuses on a comparative analysis of LST retrieved from Landsat Level 1 and Level 2 data to assess differences of the LST. Pathumthani Province, a rapidly urbanizing area in Thailand, was selected as the study site due to its dynamic land use changes and increasing thermal variability. This is the extension of the previous study conducted by [13] where the province was selected as the study area.

### *2.1 Study Area*

Pathumthani Province is located in the central region of Thailand (Figure 1), approximately 40 kilometers north of Bangkok. It lies within the Chao Phraya River basin and is part of the Bangkok Metropolitan Region, making it a key peri-urban zone experiencing rapid urbanization and industrial development. The province covers an area of around 1,500 square kilometers and comprises both urban and rural landscapes, including residential zones, agricultural fields, industrial estates, and green spaces [20]. Pathumthani has undergone significant land use and land cover (LULC) changes in recent decades, driven by population growth, infrastructure expansion, and economic development. The presence of major infrastructure such as the Navanakorn and Bangkadi industrial zones, several universities, and the extension of the mass rapid transit (MRT) system has accelerated urban sprawl, particularly along the northern and southern corridors [21].

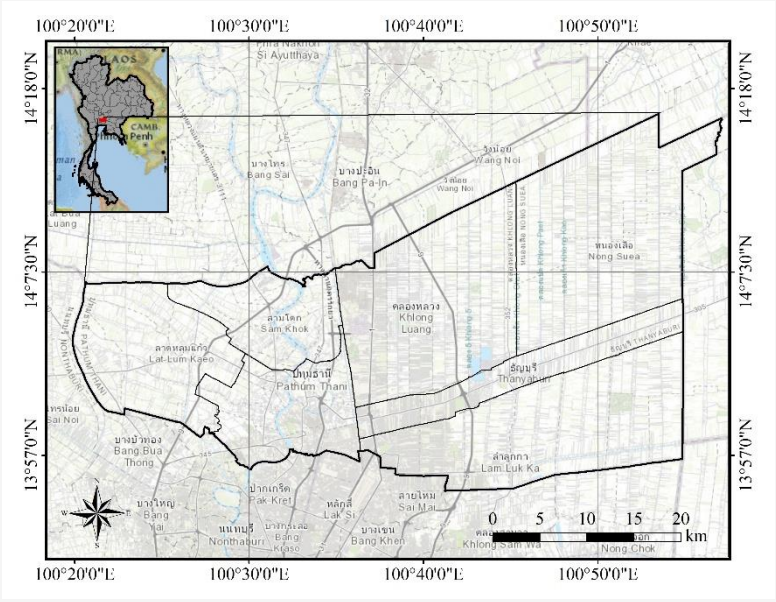


**Figure 1**: Pathumthani province, Thailand

**Table 1**: Summary of Landsat imagery used for LST analysis in Pathumthani province

| Year | Acquisition dates | Landsat Series | Spectral bands used |
|---|---|---|---|
| 2004 | 26 March 2004 | Landsat 5 TM | B3, B4, B6 |
| 2012 | 11 May 2012 | Landsat 5 TM | B3, B4, B6 |
| 2018 | 18 April 2018 | Landsat 7 ETM+ | B3, B4, B6 |
| 2023 | 18 May 2023 | Landsat 8 OLI/TIRS | B4, B5, B10 |
| 2025 | 7 January 2025 | Landsat 9 OLI/TIRS | B4, B5, B10 |

The province's mix of built-up areas, vegetation, and water bodies makes it an ideal case for analyzing spatial and temporal variations in Land Surface Temperature (LST).

*2.1 Data Used*

Landsat imagery from multiple years was processed to extract LST using standard remote sensing techniques. For Level 1 data, LST was derived using the radiative transfer equation and NDVI-based emissivity estimation, while Level 2 data provided pre-processed surface temperature outputs. The Landsat satellite imagery used in this study presents in Table 1. Landsat series 5, 7, 8, and 9 imageries were used, the red, near infrared, and thermal bands were used in the LST determination. The data were provided by the United States Geological Survey (USGS) at https://earthexplorer.usgs.gov/. Both Landsat Collection 2 Level-1 and Level-2 datasets were downloaded and utilized for the analysis. Landsat Collection 2 is the second major reprocessing of the entire Landsat archive by the United States Geological Survey (USGS), providing improved geolocation, radiometric calibration, and metadata consistency. Within Collection 2, Landsat data are categorized into Level-1 and Level-2 products as follows:

Landsat Collection 2 Level-1 products are radiometrically and geometrically corrected satellite images that serve as the foundational input for further processing. These images provide top-of-atmosphere (TOA) reflectance or radiance and are corrected for terrain and sensor geometry using precision and terrain correction (L1TP). While Level-1 data are suitable for basic visualization and general analysis, they require additional atmospheric correction and emissivity estimation before they can be used for surface-level studies, such as calculating land surface temperature (LST) or vegetation indices with high accuracy [22].

Landsat Collection 2 Level-2 products are science-ready datasets that include atmospherically corrected surface reflectance and surface temperature. These products are derived from Level-1 data using standardized processing algorithms that account for atmospheric conditions, such as water vapor, aerosols, and gases.

Level-2 data are ideal for immediate use in scientific applications, including land cover classification, climate studies, and environmental monitoring. However, their availability is subject to

certain quality conditions, such as limited cloud cover, and they are only produced for data acquired by specific Landsat missions (Landsat 4-5 TM, 7 ETM+, and 8–9 OLI/TIRS) [23].

*2.2 Study Workflow*

A consistent workflow in Figure 2 was applied for classification, calibration, and comparison to ensure meaningful evaluation between the two data levels. This section outlines the data sources, image preprocessing, LST retrieval techniques, and analytical methods used to assess spatial and temporal differences in temperature patterns across the study area. According to Figure 2, the methodology for LST determination using Landsat imagery involves several key processing steps. First, thermal infrared (TIR) data from Landsat imagery are acquired, and the digital numbers (DN) are converted to top-of-atmosphere radiance ($L_\lambda$) using scaling factors provided in the metadata. This radiance is then converted into brightness temperature (*BT*) to estimate the temperature at the sensor level. To account for surface characteristics, the Normalized Difference Vegetation Index (NDVI) is calculated using the red and near-infrared bands, which is then used to estimate the proportion of vegetation cover (*Pv*). Based on this, land surface emissivity ($\varepsilon$) is determined, assuming a mixture of vegetation and soil cover. Finally, the brightness temperature is corrected using the emissivity value to derive the actual land surface temperature [24]. This process allows for more accurate surface temperature estimation by incorporating atmospheric and surface characteristics into the analysis. The Land Surface Temperature (LST) was determined using both Level-1 and Level-2 Landsat data, and the differences between the LST values derived from the two products were subsequently analyzed.

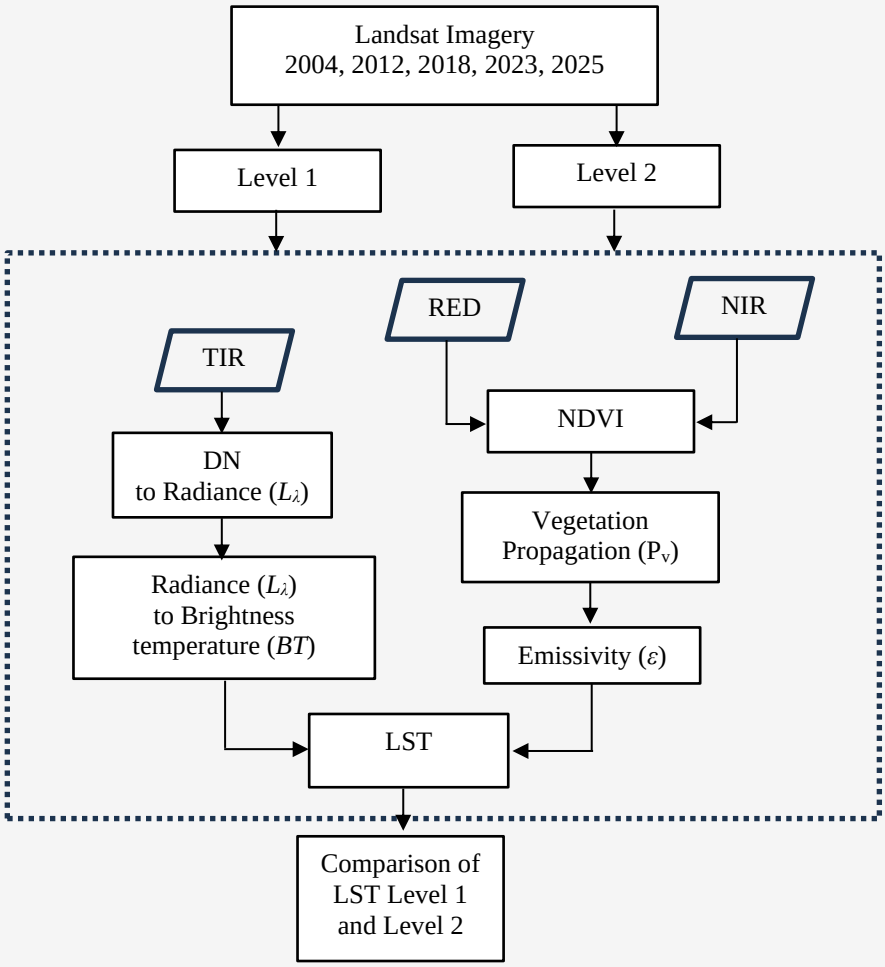


**Figure 2**: Comparison of LST derived from Landsat level 1 and 2

**Table 2**: Parameters for determining TOA spectral radiance for Landsat 4, 5, and 7

| Landsat | Band | $LMIN_\lambda$ | $LMAX_\lambda$ | $Q_{cal}MIN$ | $Q_{cal}MAX$ |
|---|---|---|---|---|---|
| Landsat 5 TM | B6 | 1.238 | 15.303 | 1 | 255 |
| Landsat 7 ETM+ | B6 VCID2 | 3.20 | 12.65 | 1 | 255 |

**Table 3**: Scaling factor for Landsat L1

| Landsat | Band | $A_L$ | $M_L$ |
|---|---|---|---|
| Landsat 5 TM | B6 | 1.18243 | 0.55375 |
| Landsat 7 ETM+ | B6 VCID2 | 3.16280 | 0.037205 |
| landsat 8 OLI/TIR | B10 | 0.10 | 0.0003342 |
| Landsat 9 OLI/TIR | B10 | 0.10 | 0.00038 |

**Table 4**: Thermal conversion constant

| Landsat series | $K_1$ (W/(m²·rad·µm)) | $K_2$ (Kelvin) |
|---|---|---|
| Landsat 5 TM | 607.79 | 1,260.56 |
| Landsat 7 ETM+ | 666.09 | 1,282.71 |
| landsat 8 OLI/TIR | 774.8853 | 1,321.0789 |
| Landsat 9 OLI/TIR | 799.0284 | 1,329.2405 |

2.*3 Data Processing*

The data processing phase involved a series of steps to prepare and analyze Landsat imagery for LST retrieval and comparison. Both Level-1 and Level-2 datasets from the Landsat Collection 2 archive were used, covering selected acquisition dates for the study area in Pathumthani Province, Thailand (Table 1). Preprocessing of Level-1 data included the following steps.

*Step 1:* Convert Digital Numbers (DN) to Top-of-Atmosphere (TOA) Radiance ($L_\lambda$) for Landsat 4, 5, and 7 using Equations 1 [25].

$$L_\lambda = \left( \frac{LMAX_\lambda - LMIN_\lambda}{Q_{cal}MAX - Q_{cal}MIN} \right) (Q_{cal} - Q_{cal}MIN) + LMIN_\lambda$$

Equation 1

Where:

$L_\lambda$ = TOA spectral radiance
$LMAX_\lambda$ = Maximum spectral radiance
$LMIN_\lambda$ = Minimum spectral radiance
$Q_{cal}$ = Quantized calibrated pixel value (DN)
$Q_{cal}MIN$ = Quantized calibrated minimum value

In case Landsat 8 and 9 imagery was used, the conversion of Digital Numbers (DN) to Top-of-Atmosphere (TOA) Radiance (Lλ) can be determined using Equations 2.

$$L_\lambda = M_L Q_{cal} + A_L$$

Equation 2

Where:

$L_\lambda$ = TOA spectral radiance
$M_L$ = Radiance multiplicative scaling factor (RADIANCE_MULT_BAND_x)
$A_L$ = Radiance additive scaling factor (RADIANCE_ADD_BAND_x)
$Q_{cal}$ = Quantized calibrated pixel value (DN)

The values of $M_L$ and $A_L$ can be found in the Landsat metadata (MTL file) which is summarized in Table 2. The additive and multiplicative scaling factors listed in Table 3 are commonly used to convert digital numbers (DN) to spectral radiance for Landsat 8 and 9. However, these scaling factors can also be applied to other Landsat series, including Landsat 4, 5, and 7. Therefore, Equation 2 can be used interchangeably with Equation 1 and offers a simplified approach for determining Land Surface Temperature (LST) from the thermal infrared band of Landsat imagery.

*Step 2:* Convert TOA Radiance to Brightness Temperature (*BT*) by apply the Planck's thermal in Equation 3.

$$BT = \frac{K_2}{\ln\left[\frac{K_1}{L_\lambda} + 1\right]} - 273.15$$

Equation 3

Where:

*BT* is at sensor brightness temperature in Celsius degree
$K_1$ and $K_2$ are thermal calibration constants from metadata (summarized in Table 4)

*Step 3:* Calculate Normalized Difference Vegetation Index (NDVI)

Vegetation plays a key role in the estimation of LST. To evaluate vegetation cover and condition, the NDVI is commonly used. NDVI reflects vegetation health by analyzing the difference in reflectance between the near-infrared (NIR) and red (RED) spectral bands [26] and [27], which are influenced by the structure of plant cells [28]. The index is computed using Equation 4.

$$NDVI = \frac{NIR - RED}{NIR + RED}$$

Equation 4

*Step 4:* Estimate Proportion of Vegetation ($P_v$)

Vegetation proportion ($P_v$) represents the fraction of a given area that is occupied by plant cover. It serves as a quantitative measure to evaluate the amount of vegetation present within a specific region. This metric is widely used in the analysis and monitoring of vegetation across various landscapes and ecosystems. $P_v$ is calculated using Equation 5 [28].

$$P_v = \left( \frac{NDVI - NDVI_{\min}}{NDVI_{\max} - NDVI_{\min}} \right)^2$$

Equation 5

Where $NDVI_{max}$ and $NDVI_{min}$ represent the maximum and minimum of NDVI, respectively.

*Step 5:* Estimate Land Surface Emissivity ($\varepsilon$)

Land surface emissivity (ε) plays a vital role in LST analysis, as it defines how efficiently a surface emits thermal radiation. In thermal infrared remote sensing, all objects with temperatures above absolute zero emit electromagnetic radiation, and the rate of this emission is influenced by the surface's emissivity. Since emissivity affects the precision of temperature values derived from thermal infrared data, it is essential for accurate LST estimation. Emissivity values vary across different surface types and typically range from 0 to 1, where a value of 1 indicates a perfect emitter (blackbody), and 0 indicates a perfect reflector. Understanding emissivity is especially important when assessing temperature differences across various land cover types and landscapes. Several models have been developed to estimate land surface emissivity using NDVI [30][31] and [32]. The NDVI Threshold method ($NDVI^{THM}$) was proposed to estimate the emissivity from NDVI [33][34][35] and [36]. The determination of emissivity depends on the NDVI values as presented in Table 5.

According to Table 5, $\varepsilon_v$ and $\varepsilon_s$ are the emissivity of vegetation and soil, respectively. The term $d_\varepsilon$ accounts for both the geometric arrangement of natural surfaces and the influence of internal reflections. While this factor can be neglected for smooth, uniform surfaces, however, for irregular or complex surfaces such as forests, it can become significant up to approximately 2% [37]. An effective estimation of this term can be expressed by Equation 6.

$$d_\varepsilon = (1 - \varepsilon_s)(1-P_v)F_{\varepsilon v}$$

Equation 6

Where: $F$ is a shape factor, which is assumed to have the mean value of 0.55 [38].

When combine the emissivity for $0.2 \leq NDVI \leq 0.5$ in Table 5 with the shape factor in equation 6. The emissivity is defined in Equation 7.

$$\varepsilon = mP_v + n$$

Equation 7

Where:

$$m = \varepsilon_v - \varepsilon_s - (1 - \varepsilon_s) F_{\varepsilon v}$$

Equation 8

$$n = \varepsilon_s + (1 - \varepsilon_s) F_{\varepsilon v}$$

Equation 9

To calculate land surface emissivity, the emissivity values for both soil and vegetation are required. A commonly accepted value of 0.99 is used for vegetation. However, selecting an appropriate soil emissivity is more challenging due to its greater variability compared to vegetation. One approach is to use the average emissivity from soil samples available in the ASTER spectral library (http://asterweb.jpl.nasa.gov), filtered using the TM6 band response function.

**Table 5**: Emissivity for different NDVI [28]

| NDVI | Emissivity ($\varepsilon$) | Land cover type |
|---|---|---|
| < 0.2 | Red band reflectivity | Bare soil |
| $0.2 \leq NDVI \leq 0.5$ | $\varepsilon_v P_v + \varepsilon_s(1-P_v) + d_\varepsilon$ | Bare soil mixed with vegetation |
| > 0.5 | 0.99 | Fully vegetated |

Based on an analysis of 49 soil spectra, the average soil emissivity is found to be 0.973, with a standard deviation of 0.004. Using these representative values 0.97 for soil and 0.99 for vegetation. The final equation for the emissivity can be derived from Equation 6 [39].

$$\varepsilon = 0.004P_v + 0.986$$

Equation 10

This equation assumes a linear combination of soil and vegetation emissivity values and is widely used in LST determination due to its lower complexity compared to other algorithms, such as the Mono-window [40] for TM data, split-window methods [41], and single channel [42].

Step 7: The brightness temperature (*BT*) can be converted to LST in the unit of Celsius degree using Equation 11.

$$LST = \frac{BT}{1 + \left[\lambda \frac{BT}{\rho}\right] Ln(\varepsilon)}$$

Equation 11

Where:

$\lambda$ is central wavelength of Landsat thermal band

$\rho$ is the constant value of $1.438 \times 10^{-2}$ mK

The LST in the unit of Celsius degree can be determined from L2 data using Equation 12 [43].

$$LST = 0.00341802 Q_{TIR} + 149 - 273.15$$

Equation 12

Where: $Q_{TIR}$ is the Quantized calibrated pixel value (*DN*) of Landsat thermal band.

The Land Surface Temperature (LST) of Pathum Thani was derived using Landsat 5, 7, 8 and 9 Collection 2 Level 1 and Level 2 data. The estimation of LST is based on the radiance values obtained from the thermal band of the Landsat sensor. Traditionally, radiance for Landsat 4, 5, and 7 is calculated using equation 1, whereas equation 2 is typically employed for Landsat 8 and 9. However, equation 2 can also be applied to Landsat 4, 5, and 7 data. This equation utilizes multiplicative and additive scaling factors, which are available in the satellite imagery metadata (MTL file). Although prior studies have commonly used equation 1 for calculating radiance in LST retrieval from Landsat 4, 5, and 7, the present study also adopts equation 2 due to its relative simplicity. Specifically, equation 2 was used to calculate the radiance of thermal band 6 (B6) for subsequent LST computation. As a result, three LST output maps were produced for Landsat 5 and 7: (1) LST derived from Level 1 data using Equation 1 for top-of-atmosphere (TOA) radiance computation (L1E1); (2) LST derived from Level 1 data using Equation 2 (L1E2); and (3) LST derived from Level 2 data using Equation 12 (L2E12).

## 3. Results and Discussion

### *3.1 LST Retrieved from Landsat 5 TM*

The retrieving LST for Pathum Thani on 26 March 2004 using Landsat 5 TM Collection 2 Level 1 and Level 2 data is depicted in Figure 3. Figure 3 clearly demonstrates that high LST values were observed in urban areas. Despite the use of different equations to determine top-of-atmosphere (TOA) radiance, the LST maps derived from the Level 1 (L1) product exhibit similar spatial distribution patterns. The maximum and minimum LST values in Figures 3(a) and 3(b) do not differ significantly. Although the LST retrieved from the L2 product also indicates higher temperatures in urban areas which consistent with the L1-derived results, however, the LST values in Figure 3(c) are notably higher than those derived from the L1 product. The spatial distribution of the LST differences between Figure 3(c) and Figure 3(a) is presented in Figure 4.

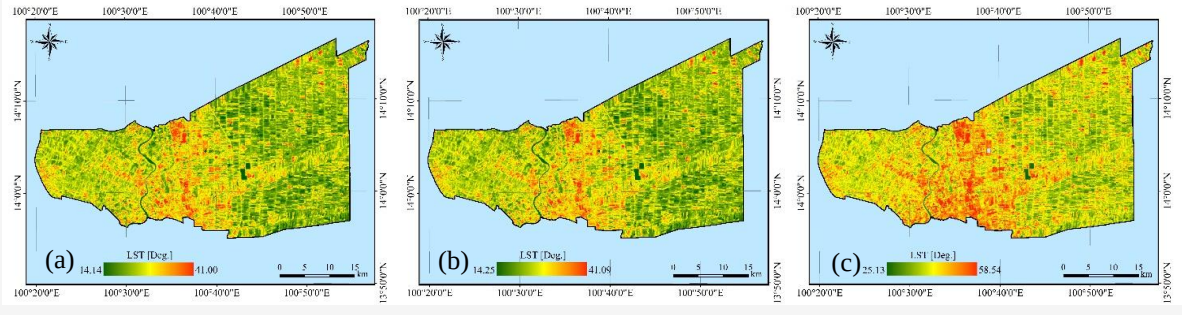


**Figure 3**: LST retrieved from Landsat 5 in 2004 (a) L1E1 (b) L1E2 (c) L2E12

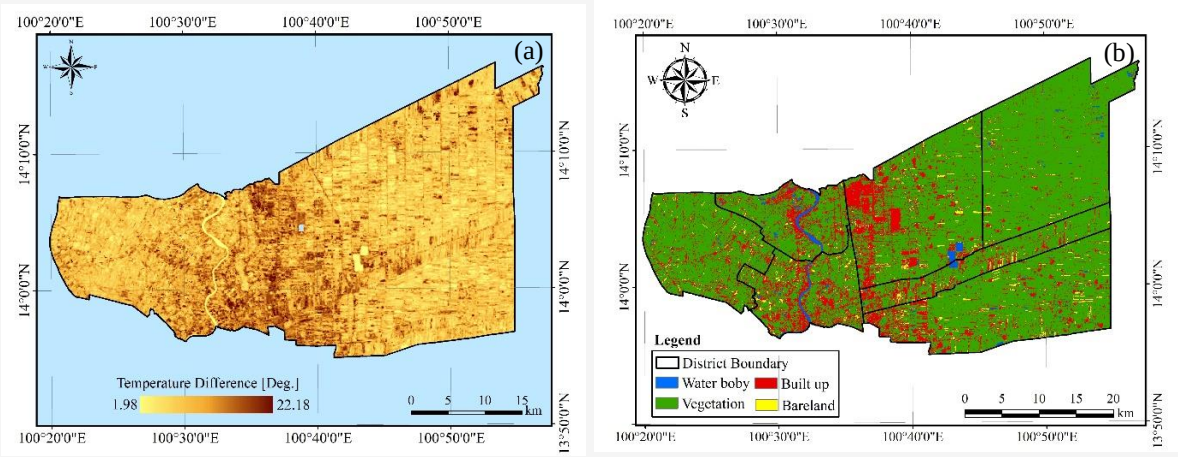


**Figure 4**: (a) LST difference between L2 and L1 product (b) LULC in 2004

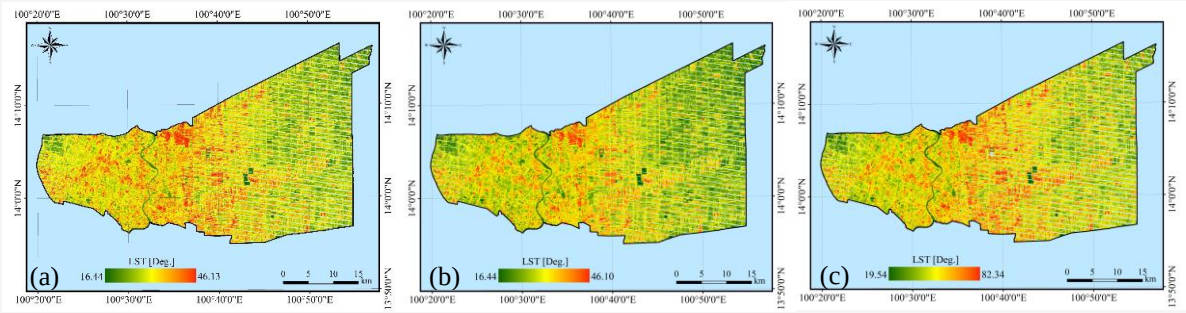


**Figure 5**: LST retrieved from Landsat 7 in 2012 (a) L1E1 (b) L1E2 (c) L2E12

Figure 4 illustrates that areas exhibiting large differences in LST between the L2 and L1 products are predominantly located in urban regions, whereas smaller differences are observed in water bodies and vegetated areas. The maximum and minimum LST differences are 22.18 °C and 1.98 °C, respectively.

*3.2 LST Retrieved from Landsat 7 ETM+*

The retrieving LST for Pathum Thani on 18 April 2018 using Landsat 7 ETM+ Collection 2 Level 1 and Level 2 data is depicted in Figure 5. The spatial distribution of LST in Pathum Thani in 2012 exhibits a similar pattern to that observed in 2004, with high LST values predominantly concentrated in urban areas. LST derived from the L1 product using different methods for calculating top-of-atmosphere (TOA) radiance, specifically, equations 1 and 2 shows no significant variation, as the minimum LST values are identical and the maximum LST values differ by only 0.03 °C. The maximum and minimum LST values retrieved from Landsat 7 imagery L1 are approximately 46.1 °C and 16.4 °C, respectively. Additionally, the overall spatial patterns of LST derived from the L1E1 and L2E12 methods are broadly similar. However, substantial differences in LST between the L2 and L1 products are observed throughout the study area. The spatial distribution of these LST differences is presented in Figure 6. It is evident that zones with high LST differences between the L2 and L1 products are primarily located in urban areas. The maximum LST difference observed is 36.22 °C, while the minimum difference of 2.20 °C occurs in water bodies. This pattern is consistent with the results from the Landsat 5 dataset; however, the magnitude of LST differences is significantly greater for Landsat 7. As shown in Figure 5(c), the maximum LST retrieved from the L2 product reaches 82.34 °C in an urban area. Given that LST derived from satellite imagery represents the skin temperature of the Earth's surfac, reflecting the temperature of land, vegetation, buildings, and other surface features such an extreme temperature value appears unrealistic and raises concerns regarding the reliability of the L2-derived LST. Furthermore, although the minimum LST derived from the L1 product is lower than that from the L2 product, the value of 16.44 °C over a water body is unexpectedly low, considering that the imagery was acquired during the summer season. Therefore, the accuracy of the LST derived from L1 data using the NDVI threshold method, particularly for water bodies, is also questionable.

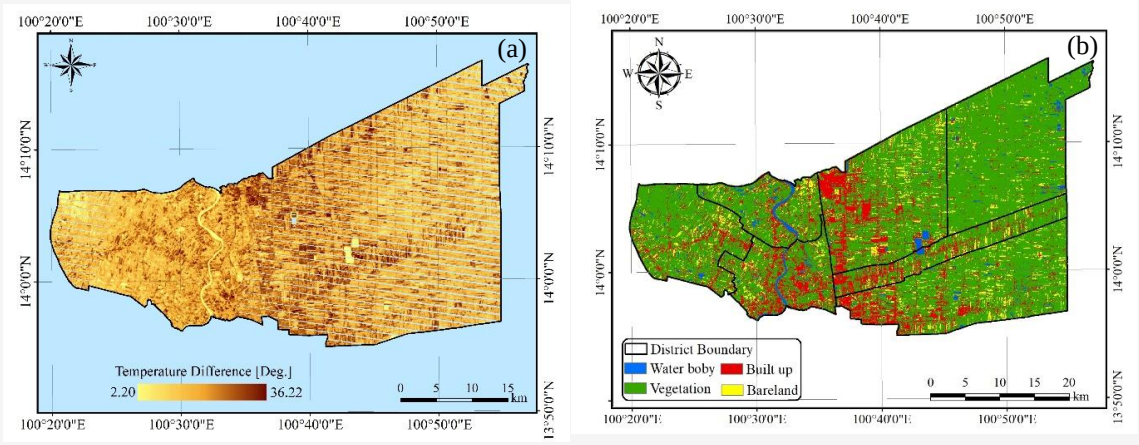


**Figure 6**: (a) LST difference between L2 and L1 product (b) LULC in 2012

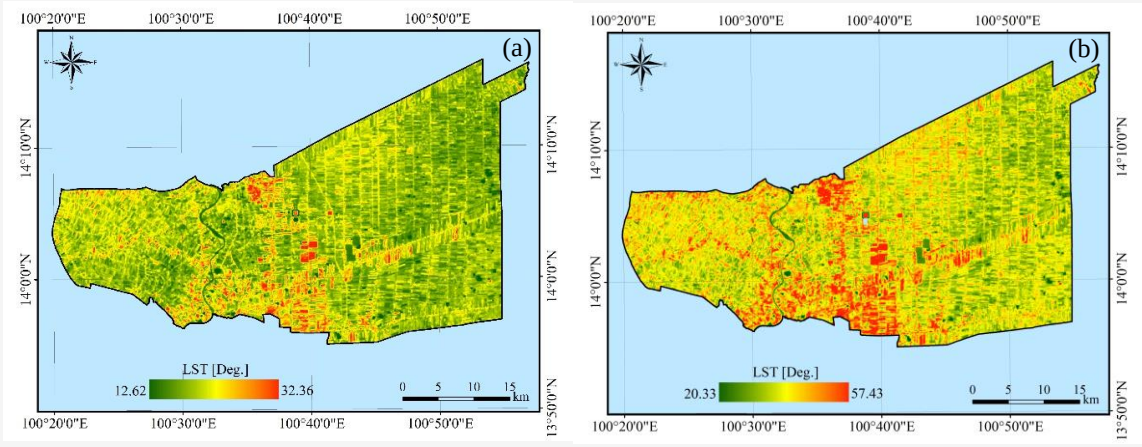


**Figure 7**: LST retrieved from Landsat 8 in 2018 (a) L1E2 (b)L2E12

*3.3 LST Retrieved from Landsat 8 OLI/TIRS*

The retrieving LST for Pathum Thani on 18 April 2018 using Landsat 8 OLI/TIRS Collection 2 Level 1 and Level 2 data is depicted in Figure 7. As illustrated in Figure 7, the LST retrieved from Landsat 8 L1 and L2 products shows a significant difference. Although high LST values are consistently observed in urban areas, the L2-derived LST is substantially higher than that obtained from the L1 data. When using the L2 product, extensive high-temperature zones are clearly visible across urban areas, whereas the L1-derived LST indicates elevated temperatures in only certain parts of the urban landscape. The maximum LST values retrieved from the L1 and L2 products are 32.36 °C and 57.43 °C, respectively. The spatial distribution of LST differences between the two products is presented in Figure 8.

The LST differences between the L2 and L1 products, as shown in Figure 8, indicate that high discrepancy zones are primarily located in urban areas, while lower differences are observed over water bodies which consistent with the patterns identified for Landsat 5 and 7. The maximum and minimum LST differences are 25.68 °C and 4.93 °C, respectively. Although the maximum LST value of 57.43 °C retrieved from the L2 product may appear plausible, it raises concerns in the context of the 2018 La Niña event. According to [13], the year 2018 recorded the lowest average LST among the study years, suggesting that such an extreme temperature may be unrealistic. This casts doubt on the reliability of the L2-derived LST, particularly for urban heat assessments and Urban Heat Island (UHI) studies. While the L1-derived LST obtained using the NDVI threshold method appears more reasonable, however, the minimum value of 12.62 °C over water bodies is unexpectedly low. This suggests that the NDVI threshold method for emissivity estimation may not be suitable for accurately retrieving LST in aquatic environments, as it tends to underestimate surface temperatures in such areas.

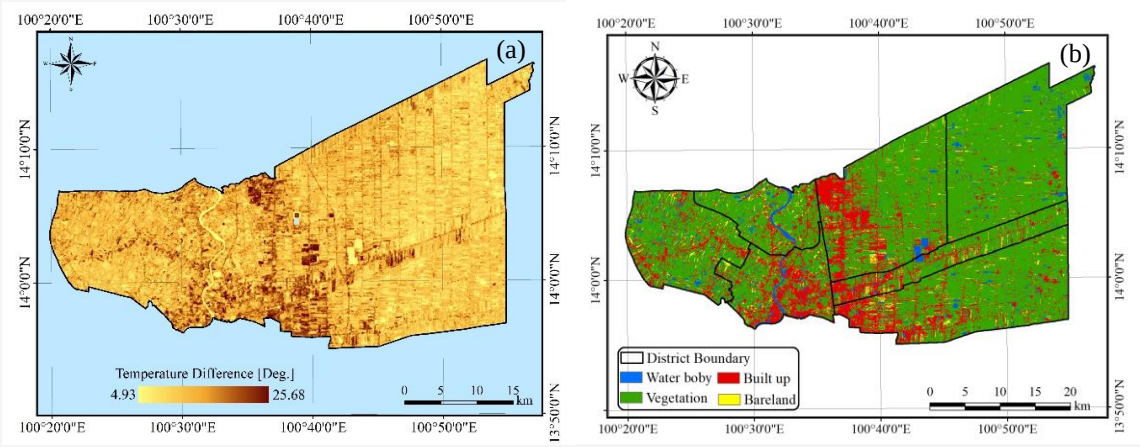


**Figure 8**: (a) LST difference between L2 and L1 product (b) LULC in 2018

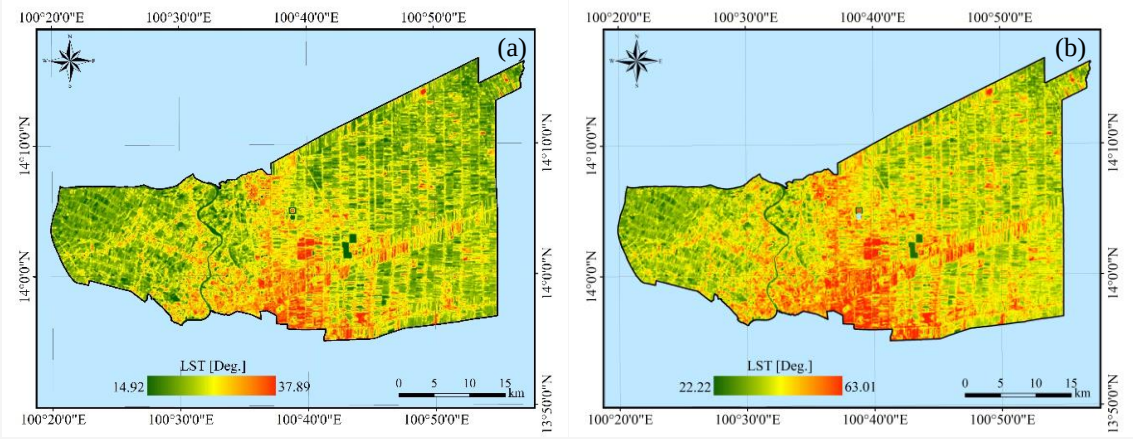


**Figure 9**: LST retrieved from Landsat 8 in 2023 (a) L1E2 (b)L2E12

*3.4 LST Retrieved from Landsat 8 OLI/TIRS*

The retrieving LST for Pathum Thani on 18 May 2023 using Landsat 8 OLI/TIRS Collection 2 Level 1 and Level 2 data is depicted in Figure 9. The results presented in Figure 9 are consistent with the observations discussed in previous sections, showing that elevated LST values are predominantly concentrated in urban areas. However, the spatial extent of high-temperature zones is considerably larger in the LST map derived from the L2 product compared to that from the L1 product. Specifically, the maximum LST recorded using the L2 product was 63.01 °C, whereas the L1-derived LST peaked at a significantly lower value of 37.89 °C. This marked discrepancy suggests a potential overestimation of surface temperatures by the L2 product or, alternatively, a possible underestimation by the L1 product, especially in densely built-up urban environments where surface emissivity and atmospheric correction errors may be more pronounced. The spatial distribution of these differences in LST between the L2 and L1 products is further illustrated in Figure 10, emphasizing the need for cautious interpretation of LST values depending on the data source and land cover characteristics.

The LST values derived from Landsat 8 L2 and L1 products are particularly evident in urban areas, especially in the southern region of the study area. The greatest discrepancy in LST was observed in urban environments, where the maximum difference reached 27.73°C. Conversely, the minimum difference of 4.85°C occurred over water bodies. This spatial pattern of LST differences is consistent with the findings discussed in the previous section. Notably, the maximum LST derived from the L2 product was 63.01°C, which is unrealistically high for urban surface temperatures. Such a value exceeds the typical upper thermal threshold of 40°C to 50°C, beyond which the human body's physiological systems begin to fail to function optimally [44].

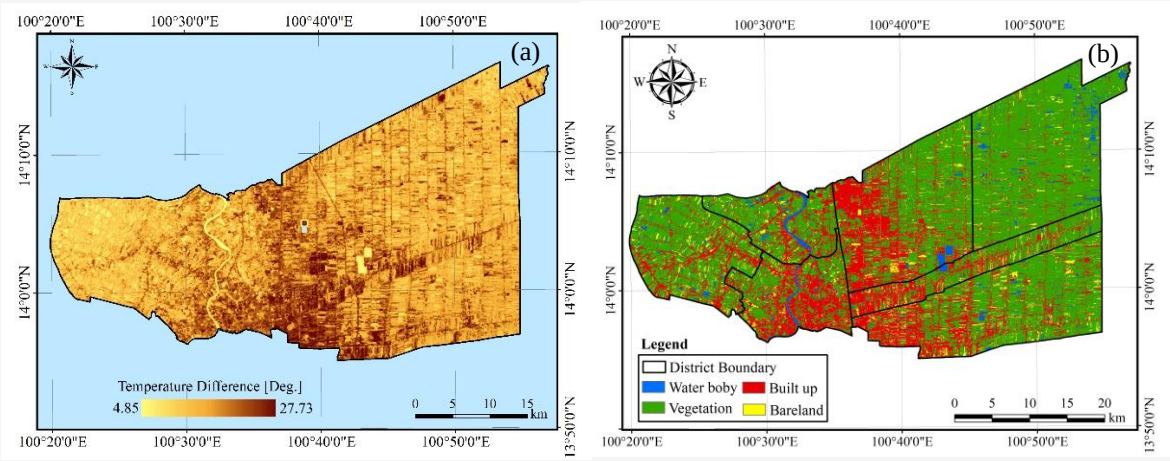


**Figure 10**: (a) LST difference between L2 and L1 product (b) LULC in 2023

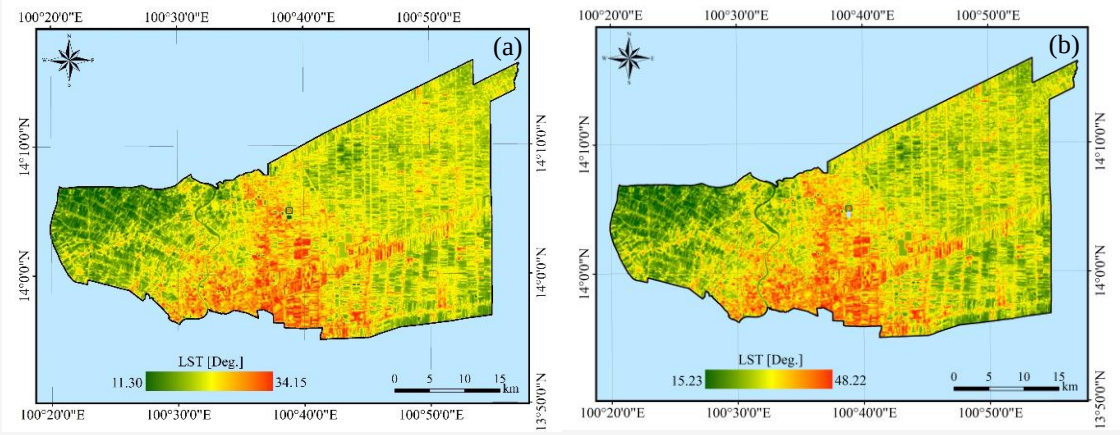


**Figure 11**: LST retrieved from Landsat 9 in 2025 (a) L1E2 (b) L2E12

This suggests that the L2 product may significantly overestimate LST in urban settings, making it unsuitable for accurate thermal characterization in these environments. In contrast, the maximum LST derived from the L1 product was 37.89°C, a value more consistent with expected surface temperatures in urban areas during the summer season.

However, while the L1 product appears to offer more plausible maximum LST values for urban areas, it may underestimate surface temperatures over water bodies. Specifically, the minimum LST derived from the L1 product was 14.92°C, which is considered uncharacteristically low for a summer season in this geographic region. Such an anomaly suggests that the L1 product may not adequately capture the thermal properties of aquatic surfaces. Figures 9 and 10 further illustrate these discrepancies. The L2-derived LST values for urban areas appear to be substantially overestimated and therefore may not provide reliable data for urban thermal analysis. In contrast, the L2 product yields more reasonable LST estimates for water bodies, implying that its application may be more suitable for non-urban, especially aquatic, environments.

*3.5 LST Retrieved from Landsat 9 OLI/TIRS*

The retrieving LST for Pathumthani on 7 January 2025 using Landsat 9 OLI/TIRS Collection 2 Level 1 and Level 2 data is depicted in Figure 11. Due to persistent high cloud cover over the study area during the hot season (March to May), it was not possible to acquire usable Landsat 9 imagery for that period. Consequently, data from January representing the cold season was used to analyze LST differences. As shown in Figure 11, the spatial distribution patterns of LST derived from both the L1 and L2 products are largely identical. High LST values are primarily concentrated in urban areas, particularly in the southern portion of the study area, which connects to Bangkok, the capital city of Thailand. High LST zones were also observed along major built-up corridors, such as the Rangsit-Makornnayok Road.

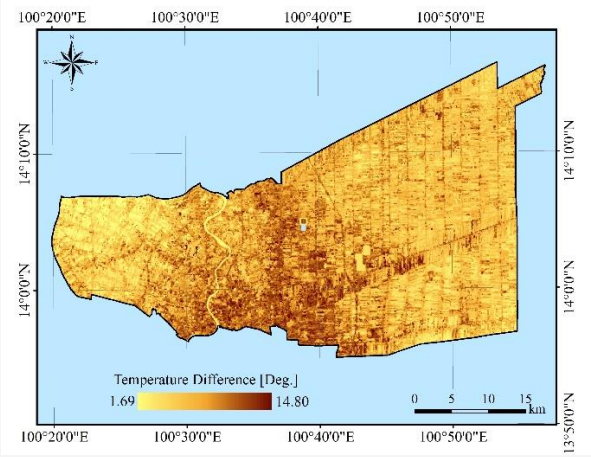


**Figure 12**: LST difference between L2 and L1 product in 2025

Despite the similar spatial distribution patterns, there are notable differences in the range of LST values obtained from the two product levels. The maximum LST derived from the L2 product was 48.22°C, which is considerably higher than the maximum of 34.15°C recorded using the L1 product. Likewise, the minimum LST values differed, with the L1 product showing a low of 11.30°C, compared to 15.23°C from the L2 product. These discrepancies suggest potential inconsistencies in the radiometric or atmospheric correction processes applied to each data level. The differences in LST values between the two product levels are further illustrated in Figure 12. Figure 12 demonstrates that the largest discrepancies in LST between the L2 and L1 Landsat products are predominantly observed in urban areas. The maximum LST difference recorded was 14.80°C, while the minimum difference, found over water bodies, was 1.69°C. When compared with earlier analyses, this case based on Landsat 9 imagery exhibits the lowest maximum LST difference. This reduction is likely attributable to the fact that the imagery was acquired during the cold season (January), when overall surface temperatures are lower and less variable, thereby reducing discrepancies between the two products.

Despite being acquired during the cold season, the maximum LST derived from the L2 product was 48.22°C, a value considered unrealistically high for this time of year. In contrast, the maximum LST from the L1 product was 34.15°C, which is more consistent with expected winter surface temperatures in the region. Regarding the minimum LST values, the lowest temperatures were observed over water bodies. The L1-derived minimum was 11.30°C, which is unusually low and may reflect an underestimation, while the L2-derived minimum of 15.23°C appears more plausible. These results mirror patterns found in previous cases: the L2 product tends to overestimate LST in urban areas, while the L1 product, particularly when applying the NDVI threshold method, tends to underestimate LST over water bodies. Therefore, careful selection of the appropriate Landsat data product is essential for accurate LST estimation and should be guided by the land use/land cover (LULC) characteristics of the study area. Specifically, the L2 product may not be suitable for urban thermal studies due to its tendency to overestimate high-temperature zones, whereas the L1 product with NDVI-based corrections may be less reliable over water surfaces.

### *3.6 Comparison of the LST Retrieved from L1 and L2 Products*

The comparison of LST values derived from the Level-1 (L1) and Level-2 (L2) Landsat products is statistically summarized in Table 6. The Land Surface Temperature (LST) values derived from L1 products using Top of Atmosphere (TOA) radiance calculated through equation 1 for Landsat 5 and Landsat 7 do not significantly differ from those obtained using equation 2. Specifically, the differences in maximum LST values were 0.09°C for Landsat 5 and 0.03°C for Landsat 7, while the differences in minimum values were 0.11°C for both sensors. The discrepancies in mean LST were 0.10°C for Landsat 5 and 0.01°C for Landsat 7. Additionally, the standard deviation of LST values derived from both equations was identical, indicating similar variability in the outputs. These results suggest that equation 2, which incorporates a scaling factor, can accurately estimate thermal band radiance (Band 6) for both sensors. This radiance can subsequently be used to compute brightness temperature (*BT*) and then converted to LST. Given its computational simplicity and comparable accuracy, equation 2 presents a more efficient alternative to Equation 1 for TOA radiance calculations in LST retrieval.

**Table 6**: The comparison of LST retrieved from L1 and L2 Landsat products

| Satellite | Acquisition dates | Max.LST [°C] | | Min.LST [°C] | | Avg.LST [°C] | | Std.LST [°C] | |
|---|---|---|---|---|---|---|---|---|---|
| | | L1 | L2 | L1 | L2 | L1 | L2 | L1 | L2 |
| Landsat 5 | 26 March 2004 | *41.00 | 58.54 | *14.14 | 25.13 | 29.19 | 36.82 | 1.53 | 3.14 |
| | | **41.09 | | **14.25 | | 29.29 | | 1.53 | |
| Landsat 7 | 11 May 2012 | *46.13 | 82.34 | *16.44 | 19.54 | 26.92 | 42.26 | 1.81 | 4.08 |
| | | **46.10 | | **16.44 | | 26.91 | | 1.81 | |
| Landsat 8 | 18 April 2018 | 32.36 | 57.43 | 12.62 | 20.33 | 23.06 | 34.82 | 1.15 | 2.53 |
| Landsat 8 | 18 May 2023 | 37.89 | 63.01 | 14.92 | 22.22 | 28.43 | 43.58 | 1.73 | 3.60 |
| Landsat 9 | 7 January 2025 | 34.14 | 48.22 | 11.30 | 15.28 | 24.97 | 30.30 | 1.89 | 2.95 |

Remark: * denotes radiance determined from equation 1.
** denotes radiance determined from equation 2.

Further analysis of LST variability shows that the L1-derived LST exhibits an average standard deviation of approximately 1.63°C, with a maximum of 1.89°C and a minimum of 1.15°C. In contrast, the L2-derived LST displays a significantly higher average standard deviation of 3.26°C, ranging from 2.53°C to 4.08°C. A lower standard deviation indicates that the LST values are more tightly clustered around the mean, implying greater consistency and reliability. Therefore, the lower variability observed in the L1-derived LST suggests it offers more stable and uniform temperature estimates across different spatial and temporal scales, supporting its reliability for applications requiring precision.

In this study, LST was estimated using two different approaches. For the L1 product, the NDVI threshold method was applied alongside equation 11, while equation 12 was used with scaling factors to derive LST from the L2 product. The results presented in table 6 reveal that the LST values retrieved from the L2 product are consistently higher than those from the L1 product. Notably, the maximum LST from the L2 product for Landsat 7 reached 82.34°C, which appears unrealistically high for land surface conditions, particularly in urban areas. Since LST represents the skin temperature of the Earth's surface encompassing elements such as soil, vegetation, and built-up areas, it differs substantially from air temperature, typically measured 1.5 to 2 meters above the surface. Such extreme surface temperatures would be uninhabitable for humans, especially in urban environments. Exposure to temperatures exceeding 35°C in humid conditions or 40°C in dry conditions poses severe health risks and can be fatal. With rising trends in heat event frequency, intensity, and duration, the potential for physiological stress and damage to humans, animals, and ecosystems increases considerably [45]. Therefore, the reliability of LST data derived from the L2 product in urban areas is questionable, as the results may be exaggerated. In contrast, the L1 product, when processed using the NDVI threshold method, provides more realistic and reliable LST values for urban settings. However, for aquatic environments, the L2 product yields more plausible LST values compared to the L1 product, which tends to significantly underestimate water body temperatures.

**Table 7**: The difference between L1 and L2-derived LST

| Satellite | Acquisition dates | LST(L2) – LST(L1) [°C] | | LST(Max) – LST(Min) [°C] | | Avg.LST(L2) - Avg.LST(L1) [°C] |
|---|---|---|---|---|---|---|
| | | ΔMax.LST | ΔMin.LST | L1 | L2 | |
| Landsat 5 | 26 March 2004 | 17.54 | 10.99 | 26.86 | 33.41 | 7.63 |
| | | 17.45 | 10.88 | 26.84 | | 7.53 |
| Landsat 7 | 11 May 2012 | 36.21 | 3.10 | 29.69 | 62.80 | 15.34 |
| | | 36.24 | 3.10 | 29.66 | | 15.35 |
| Landsat 8 | 18 April 2018 | 25.07 | 7.71 | 19.74 | 37.10 | 11.76 |
| Landsat 8 | 18 May 2023 | 25.12 | 7.30 | 22.97 | 40.79 | 15.15 |
| Landsat 9 | 7 January 2025 | 14.08 | 3.98 | 22.84 | 32.94 | 5.33 |

Consequently, based on these findings, the L2 product is more appropriate for estimating LST in water bodies, while the L1 product, processed with the NDVI threshold method, is more suitable for urban thermal analysis. The differences between the LST derived from these two methods presents in Table 7.

The difference between the maximum LST values derived from Level 2 (L2) and Level 1 (L1) products (ΔMax.LST) ranges from 14.08°C for Landsat 9 to 36.24°C for Landsat 7. This substantial discrepancy

indicates that higher LST values are associated with greater divergence between the two products. Consequently, it can be inferred that in high-temperature regions, such as urban areas, the L2 and L1 products yield significantly different LST estimates. Therefore, they cannot be used interchangeably for accurate LST retrieval in such environments. In terms of the minimum LST difference (ΔMin.LST), the values range from 3.10°C (Landsat 7) to 10.99°C (Landsat 5). These differences are relatively smaller compared to the maximum LST discrepancies, suggesting that the divergence between L1 and L2 products is less pronounced in cooler surface conditions. Notably, despite Landsat 7 exhibiting the highest ΔMax.LST, it also shows the lowest ΔMin.LST, highlighting an inconsistent performance across the LST spectrum.

The range of LST values (LST(Max) – LST(Min)) further emphasizes this variability. For the L1 product, the temperature range varies between 19.74°C and 29.69°C across all Landsat missions. In contrast, the L2 product exhibits significantly higher variability, particularly in Landsat 7, which shows an extreme temperature range of 62.80°C. Even the lowest LST range from the L2 product (Landsat 9, at 32.94°C) remains higher than the maximum range observed in the L1 product. These findings suggest that L2-derived LST values exhibit a higher degree of variability and include unrealistically elevated maximum temperatures that are inconsistent with real-world surface conditions. This issue is especially critical in urban areas, where accurate thermal readings are essential for environmental monitoring and public health assessment.

Furthermore, the difference in average LST between the L2 and L1 products (Avg.LST(L2) – Avg.LST(L1)) confirms these concerns. Landsat 7 shows the greatest average difference at approximately 15.3°C, while Landsat 9 records the smallest. This trend is consistent with the observed ΔMax.LST values, reinforcing the conclusion that the L2 product may overestimate surface temperatures in high-LST regions. These results collectively indicate that L2-derived LST data may not be suitable for representing urban thermal conditions due to its inflated temperature estimates and high variability. Conversely, the L1 product demonstrates greater reliability and consistency for urban LST estimation. However, the L2 product may still be appropriate for assessing water bodies, where its LST estimates appear to align more closely with expected surface conditions. The accuracy of Land Surface Temperature (LST) estimation for water bodies using Equation 11 in conjunction with the NDVI threshold method is largely influenced by surface emissivity. Emissivity is a critical parameter in thermal remote sensing, as it quantifies the efficiency with which a surface emits thermal radiation relative to an ideal blackbody, which has an emissivity value of 1.0. In practice, natural surfaces such as soil, vegetation, and water typically exhibit emissivity values ranging between 0.90 and 0.99. Equation 4 assumes a minimum emissivity of 0.986, which is generally appropriate for urban surfaces characterized by mixed land cover types such as built-up areas and vegetation.

However, when applied to water bodies, this assumed emissivity may not yield accurate LST values. If the actual emissivity of water surfaces is lower than 0.986, the resulting LST estimates will be underestimated. This issue is evident in the current results, where anomalously low LST values are consistently observed over water bodies, suggesting that the emissivity parameter used in Equation 4 may not be optimal for aquatic environments.
Such unrealistically low temperatures undermine the credibility of LST retrieval in these regions. In contrast, the LST values retrieved from Equation 12, which is applied to the Level 2 product, appear more consistent with expected thermal behavior of water surfaces. This suggests that Equation 12 may incorporate a more accurate or context-appropriate emissivity value for water bodies. Therefore, while Equation 4 may be suitable for urban LST estimation, it may not be appropriate for aquatic environments. For improved accuracy in LST retrieval over water surfaces, the use of Equation 12 is recommended, as it yields more realistic and reliable results.

The Landsat Collection 2 Level-2 Surface Temperature (ST) products are generated using the Landsat Surface Temperature Algorithm (Version 1.3.0), developed in collaboration with the Rochester Institute of Technology and NASA's Jet Propulsion

Laboratory [23]. This algorithm computes land surface temperature in Kelvin by applying atmospheric corrections to thermal infrared data from Landsat sensors, incorporating inputs such as Top of Atmosphere (TOA) reflectance, TOA Brightness Temperature, and data from the ASTER Global Emissivity Database (GED) and NDVI. L2-derived LST in this study show higher values than L1 data due to its advanced processing steps that account for atmospheric and surface conditions. L1 data represent TOA brightness temperatures, which are influenced by atmospheric absorption and scattering, often causing the observed thermal radiation to appear cooler than the actual surface temperature. In contrast, L2 data apply atmospheric corrections using radiative transfer models to remove these effects, resulting in higher LST values. Another key factor is emissivity adjustment. L1 data assume an ideal blackbody with perfect emissivity (1.0), while L2

data incorporate realistic emissivity values (ranging from 0.90 to 0.99 for natural surfaces) to correct for how different materials emit thermal radiation. This adjustment further increases L2 LST values compared to L1, particularly for surfaces like dry soil or urban areas that have lower emissivity. Additionally, L2 processing employs specialized algorithms, such as split-window or single-channel methods, which further refine temperature estimates by minimizing atmospheric interference.

## 4. Conclusion

This comprehensive study comparing Land Surface Temperature (LST) derived from Landsat Level 1 (L1) and Level 2 (L2) data products has provided critical insights into the strengths, limitations, and optimal applications of each dataset for environmental monitoring and urban thermal analysis. Drawing on a robust temporal dataset spanning from 2004 to 2025 and incorporating multiple Landsat missions (5, 7, 8, and 9) focused on Pathum Thani Province, the analysis revealed notable discrepancies between LST estimates from L1 and L2 products. One of the key findings is the consistently higher LST values derived from L2 products reaching differences of up to 36.24°C in urban areas highlighting the significant influence of atmospheric correction and emissivity modeling techniques on thermal measurements. While L2 products offer the advantage of standardized atmospheric correction and emissivity adjustments, the tendency to yield unrealistically high temperatures in urban settings such as the extreme 82.34°C observed from Landsat 7 raises concerns about potential overcorrection in automated processing algorithms. In contrast, L1-derived LST values, when calculated using NDVI-based emissivity correction methods, yielded more realistic temperature ranges in urban areas but tended to underestimate temperatures in water bodies. These contrasting patterns suggest that neither L1 nor L2 products are universally superior; rather, their suitability depends on land cover types and specific research objectives.

For urban thermal applications, L1 data, when paired with careful emissivity modeling, appears to produce more reliable results. Conversely, L2 products may be better suited for aquatic environments, where their emissivity assumptions yield more plausible thermal readings. The study also identified significant sensor-specific variations, with Landsat 7 exhibiting the greatest differences between L1 and L2-derived LST, indicating that algorithm performance is not uniform across sensor generations. This finding underscores the importance of sensor-specific calibration when conducting long-term or multi-sensor thermal analyses.

Furthermore, the temporal component of the analysis showed that seasonal variability influences the magnitude of LST discrepancies between L1 and L2 products, with smaller differences observed during cooler periods. This temporal sensitivity highlights the need to consider seasonal context in LST comparisons and reinforces the importance of integrating seasonal dynamics in future studies. In conclusion, this research demonstrates that careful selection and processing of Landsat thermal data are essential for accurate LST estimation.

## 5. Limitations

This study was confined to Pathum Thani Province, which may limit the generalizability of the findings to regions with differing climatic conditions, land use patterns, or surface characteristics. Additionally, the temporal scope of the analysis (2004-2025) did not account for seasonal variations, which are known to significantly affect land surface temperature dynamics. The absence of seasonal representation may constrain the interpretation of long-term trends and variability in LST. Moreover, the lack of sufficient ground-based LST measurements hindered the ability to perform robust validation of the satellite-derived temperature estimates, thereby limiting the assessment of absolute accuracy.

## 6. Future Works and Recommendation

Regions and incorporate seasonal variability to better understand the temporal and spatial dynamics of LST differences between Level 1 (L1) and Level 2 (L2) products. Moreover, the accuracy of satellite-derived LST should be validated using in-situ ground-based temperature measurements, such as those obtained from meteorological stations. This validation is essential to ensure the reliability of remote sensing-derived thermal data. In addition, alternative LST retrieval algorithms such as the Split Window technique or machine learning-based approaches should be explored to assess their performance relative to traditional methods and to potentially improve the accuracy of LST estimation across diverse land cover types and environmental conditions.

**References**


[1] Sekertekin, A. and Bonafoni, S., (2020). Land Surface Temperature Retrieval from Landsat 5, 7, and 8 over Rural Areas: Assessment of Different Retrieval Algorithms and Emissivity Models and Toolbox Implementation. *Remote Sensing*, Vol. 12(2). https://doi.org/10.3390/rs12020294.

[2] Sharaf El Din, E., Elsherif, A., Ramadan, S. and Aboelkhair, H., (2023). Mapping of Thermal Indices Using an Automated Landsat 8-based-ArcGIS Model: A Case Study in Alexandria City, Egypt. *International Journal of Geoinformatics*, Vol. 19(9), 1–12. https://doi.org/10.52939/ijg.v19i9.2823.

[3] Armayanti, A., Syaf, H., Dewi, Y. and Nurgiantoro, N., (2019). Analysis of Urban Heat Island Intensity Using Multi Temporal Landsat Data; Case Study of Kendari City, Indonesia. *IOP Conference Series Earth and Environmental Science*, Vol. 389. https://doi.org/10.1088/1755-1315/389/1/012002.

[4] Jaelani, L. and Handayani, C., (2022). Spatio-temporal Analysis of Land Surface Temperature Changes in Java Island from Aqua and Terra MODIS Satellite Imageries Using Google Earth Engine. *International Journal of Geoinformatics*, Vol. 18(5), 1-12. https://doi.org/10.52939/ijg.v18i5.2365.

[5] Moazzam, M. and Lee, B., (2023). Elevation-Wise and Direction-Wise Distribution of Land Surface Temperature in Jeju Island using Landsat 7 Data. *International Journal of Geoinformatics*, Vol. 19(9), 13-20. https://doi.org/10.52939/ijg.v19i9.2825.

[6] Chopra, R. and Singh, T., (2022). Urban Heat Island Studies and its Effects Across the Different Cities of the India - A Review. *International Journal of Geoinformatics*. Vol.18(2), 17-27. https://journals.sfu.ca/ijg/index.php/journal/article/view/2147.

[7] Jagtap, A., Shedge, D. and Mane, P., (2024). Exploring the Effects of Land Use/Land Cover (LULC) Modifications and Land Surface Temperature (LST) in Pune, Maharashtra with Anticipated LULC for 2030. *International Journal of Geoinformatics*. Vol. 20(2), 42-63. https://doi.org/10.52939/ijg.v20i2.3065.

[8] Abdivaitov, K., Strobl, J. and Tynybekova, A., (2023). Agricultural Land Use Dynamics - A Case Study of Kumkurgan District, Uzbekistan. *International Journal of Geoinformatics*, Vol. 19(11), 38-44. https://doi.org/10.52939/ijg.v19i11.2921.

[9] Sameh, S., Zarzoura, F. and El-Mewafi, M., (2022). Automated Mapping of Urban Heat Island to Predict Land Surface Temperature and Land Use/Cover Change Using Machine Learning Algorithms: Mansoura City. *International Journal of Geoinformatics*, Vol. 18(6), 47-67. https://doi.org/10.52939/ijg.v18i6.2461.

[10] Aldileemi, H., Zhran, M. and El-Mewafi, M., (2023). Geospatial Monitoring and Prediction of Land Use/Land Cover (LULC) Dynamics Based on the CA-Markov Simulation Model in Ajdabiya, Libya. *International Journal of Geoinformatics*, Vol. 19(12), 15-29. https://doi.org/10.52939/ijg.v19i12.2973.

[11] Mostafa, K. M., (2023). Evaluating the Spatiotemporal Dynamics of Land Surface Temperature in Relation to the Land Use/Land Cover changes in Nag-Hammadi District, Egypt, using Remote Sensing and GIS. *International Journal of Geoinformatics*, Vol. 19(3), 13-29.

[12] Ordoñez, C. A. and Silva, D., (2023). Land Use/Land Cover (LULC), change Detection, and Simulation Analysis of Manila Bay's Dolomite Mining Site in Cebu, Philippines Using Sentinel-2 Satellite. *International Journal of Geoinformatics*. Vol. 19(5), 87-103. https://doi.org/10.52939/ijg.v19i5.2667.

[13] Thammaboribal, P., (2024). Investigating Land Surface Temperature Variation and Land Use Land Cover Changes in Pathumthani, Thailand (1997-2023) using Landsat Satellite Imagery: A Comprehensive Analysis of LST and Urban Hot Spots (UHS). *International Journal of Geoinformatics*, Vol. 20(2), 27–41. https://doi.org/10.52939/ijg.v20i2.3063.

[14] Weng, O., Lu, D. and Schubring, J., (2004). Estimation of Land Surface Temperature Vegetation Abundance Relationship for Urban Heat Island Studies. *Remote Sensing of Environment*, Vol. 89(4), 467-483. https://doi.org/10.1016/j.rse.2003.11.005.

[15] Jiménez-Muñoz, J. C. and Sobrino, J. A., (2003). A Generalized Single-Channel Method for Retrieving Land Surface Temperature from Remote Sensing Data. *Journal of Geophysical Research*. Vol. 108(D22). https://doi.org/10.1029/2003JD003480.

[16] Li, H., Zhou, Y., Li, X., Meng, L., Wang, X., Wu, S. and Sodoudi, S., (2018). A New Method to Quantify Surface Urban Heat Island Intensity. *Science of the Total Environment*. Vol. 624, 262-272. https://doi.org/10.1016/j.scitotenv.2017.11.360.

[17] Teixeira Pinto, C., Jing, X. and Leigh, L., (2020). Evaluation Analysis of Landsat Level-1 and Level-2 Data Products Using in Situ Measurements. *Remote Sensing*, Vol. 12(16). https://doi.org/10.3390/rs12162597.

[18] Guo, J., Ren, H., Zheng, Y., Lu, S. and Dong, J., (2020). Evaluation of Land Surface Temperature Retrieval from Landsat 8/TIRS Images before and after Stray Light Correction Using the SURFRAD Dataset. *Remote Sensing*, Vol. 12(6). https://doi.org/10.3390/rs12061023.

[19] Chander, G., Markham, B., L. and Helder, D. L., (2009). Summary of Current Radiometric Calibration Coefficients for Landsat MSS, TM, ETM+, and EO-1 ALI Sensors. *Remote Sensing of Environment*, Vol. 113(5), 893-903. https://doi.org/10.1016/j.rse.2009.01.007.

[20] Selanon, P., Puggioni, F., Dejnirattisai, S. and Rutchamart, A., (2022). Towards Inclusive and Accessible Parks in Pathum Thani Province, Thailand. *City Territory and Architecture*, Vol. 9, 1-16. https://doi.org/10.1186/s40410-022-00169-y.

[21] Thammaboribal, P. and Tripathi, N., (2024). Predicting Land Use and Land Cover Changes in Pathumthani, Thailand: A Comprehensive Analysis from 2013 to 2023 Using Landsat Satellite Imagery and CA-ANN Algorithm, with Projections for 2028 and 2038. *International Journal of Geoinformatics*. Vol. 20(5), 13–27. https://doi.org/10.52939/ijg.v20i5.3225.

[22] Landsat Missions. (n.d.). Landsat Collection 2 level-1 Data. [Online]. Available: https://www.usgs.gov/landsat-missions/landsat-collection-2-level-1-data. [Accessed: Feb. 11, 2025].

[23] Landsat Missions. (n.d.). Landsat Collection 2 level-2 Science Products. [Online]. Available: https://www.usgs.gov/landsat-missions/landsat-collection-2-level-2-science-products. [Accessed: Feb. 11, 2025].

[24] Namwong, C., Suwanprasit, C., Shahnawaz, S. and Wongpornchai, P., (2023). Assessing the Relationship between Forest Proportion, Soil Moisture Index and Net Primary Productivity in Pa Sak Ngam, Chiang Mai Province, Thailand. *International Journal of Geoinformatics*. Vol. 19(2), 25–38. https://doi.org/10.52939/ijg.v19i2.2563.

[25] Mostafa K. M., (2023). Evaluating the Spatiotemporal Dynamics of Land Surface Temperature in Relation to the Land Use/Land Cover changes in Nag-Hammadi District, Egypt, Using Remote Sensing and GIS. *International Journal of Geoinformatics*, Vol. 19(3), 13–29. https://doi.org/10.52939/ijg.v19i3.2599.

[26] Ali, Z., Jaelani, L. and Sumargana, L., (2024). Detection of Corn Phenological Stages with Landsat Satellite Imagery: A Case Study in Ngawi Regency, Indonesia. *International Journal of Geoinformatics*, Vol. 20(9), 1-15. https://doi.org/10.52939/ijg.v20i9.3535.

[27] Samarkhanov, K., Sadenova, M. and Beisekenov, N., (2023). Analysis of Crop Spectral Reflectance at the Croplands in Eastern Kazakhstan Using Satellite Imagery. *International Journal of Geoinformatics*, Vol. 19(11), 45–53. https://doi.org/10.52939/ijg.v19i11.2923.

[28] Balew, A. and Korme, T., (2020). Monitoring Land Surface Temperature in Bahir Dar City and Its Surrounding using Landsat Images. *The Egyptian Journal of Remote Sensing and Space Science*, Vol. 23(3), 371-386. https://doi.org/10.1016/j.ejrs.2020.02.001.

[29] Carlson, T. N. and Ripley, D. A., (1997). On the Relation Between NDVI, Fractional Vegetation Cover, and Leaf Area Index. *Remote Sensing of Environment*, Vol. 62, 241-252.

[30] Sobrino, J. A. and Raissouni, N., (2000). Toward Remote Sensing Methods for Land Cover Dynamic Monitoring. Application to Morocco. *International Journal of Remote Sensing*, Vol. 21, 353-366. https://doi.org/10.1080/014311600210876.

[31] Valor, E. and Caselles, V., (1996). Mapping Land Surface Emissivity from NDVI: Application to European, African and South American Areas. *Remote Sensing of Environment*, Vol. 57, 167-184. https://doi.org/10.1016/0034-4257(96)00039-9.

[32] Van de Griend, A. A. and Owe, M., (1993). On the Relationship Between Thermal Emissivity and the Normalized Difference Vegetation Index for Natural Surfaces. *International Journal of Remote Sensing*, Vol. 14(6), 1119-1131.

[33] Sobrino, J. A., Jimenez-Muoz, J. C., Soria, G., Romaguera, M., Guanter, L., Moreno, J., Plaza, A. and Martinez, P., (2008). Land Surface Emissivity Retrieval from Different VNIR and TIR Sensors. *IEEE Transactions on Geoscience & Remote Sensing*, Vol. 46, 316–327. https://doi.org/10.1109/TGRS.2007.904834.

[34] Skokovic, D., Sobrino, J. A., Jiménez Muñoz, J. C., Soria, G., Julien, Y., Mattar, C. and Cristóbal, J., (2014). Calibration and Validation of Land Surface Temperature for Landsat8-TIRS Sensor TIRS Landsat-8 Characteristics. *Conference: ESA Land Product Validation and Evolution*. [Online]. Available: https://earth.esa.int/documents/700255/2126408/ESA_Lpve_Sobrino_2014a.pdf. [Accessed: Feb. 14, 2025].

[35] Yu, X., Guo, X. and Wu, Z., (2014). Land Surface Temperature Retrieval from Landsat 8 TIRS-Comparison between Radiative Transfer Equation-Based Method, Split Window Algorithm and Single Channel Method. *Remote Sensing*. Vol. 6, 9829–9852. https://doi.org/10.3390/rs6109829.

[36] Li, S. and Jiang, G. M., (2018). Land Surface Temperature Retrieval from Landsat-8 Data with the Generalized Split-Window Algorithm. *IEEE Access*. Vol. 6, 18149–18162. https://doi.org/10.1109/ACCESS.2018.2818741.

[37] Sobrino, J. A., (1989). *Desarrollo de un modelo teo´rico para implementar la medida de la temperatura realizada mediante teledeteccio´n. Aplicacio´n a un campo de naranjos. [Development of a Theoretical Model for Implementing Remote Sensing Temperature Measurement. Application to an Orange Grove]*. PhD dissertation, University of Valencia, Valencia, Spain.

[38] Sobrino, J. A., Caselles, V. and Becker, F., (1990). Significance of the Remotely Sensed Thermal Infrared Measurements Obtained Over a Citrus Orchard. *ISPRS Photogrammetric Engineering and Remote Sensing*. Vol. 44, 343-354. https://doi.org/10.1016/0924-2716(90)90077-O.

[39] Sobrino, J. A., Jiménez-Muñoz, J. C. and Paolini, L., (2004). Land Surface Temperature Retrieval from LANDSAT TM 5. *Remote Sensing of Environment*, Vol. 90(4), 434-440, https://doi.org/10.1016/j.rse.2004.02.003.

[40] Qin, Z., Karnieli, A. and Berliner, P. A., (2001). Mono-Window Algorithm for Retrieving Land Surface Temperature from Landsat TM Data and Its Application to the Israel-Egypt Border Region. *International Journal of Remote Sensing*. Vol. 22, 3719-3746. https://doi.org/10.1080/01431160010006971.

[41] Mao, K., Qin, Z., Shi, J. and Gong, P. A., (2005). Practical Split-Window Algorithm for Retrieving Land-Surface Temperature from MODIS Data. *International Journal of Remote Sensing*, Vol. 26, 3181–3204. https://doi.org/10.1080/01431160500044713.

[42] Jiménez-Muñoz, J. C., Cristóbal, J., Sobrino, J. A., Sòria, G., Ninyerola, M. and Pons, X., (2009). Revision of the Single-Channel Algorithm for Land Surface Temperature Retrieval from Landsat Thermal-Infrared Data. *IEEE Transactions on Geoscience & Remote Sensing*, Vol. 47, 339–349. https://doi.org/10.1109/TGRS.2008.2007125.

[43] Landsat Missions. (n.d.). Landsat Collection 2 Surface Temperature. [Online]. Available: https://www.usgs.gov/landsat-missions/landsat-collection-2-surface-temperature. [Accessed: Feb. 11, 2025].

[44] Lennon, A., (2023). How Hot is Too Hot for the Human Body? Study Offers New Insights. [Online]. Available: https://www.medicalnewstoday.com/articles/how-hot-is-too-hot-for-the-human-body-heart-metabolic-rate. [Accessed: Feb. 15, 2025].

[45] Asseng, S., Spänkuch, D., Hernandez-Ochoa, I. M. and Laporta, J., (2021). The Upper Temperature Thresholds of Life. *The Lancet Planetary Health*, Vol. 5(6), e378-385.